Catal Lett (2013) 143:1247–1254
DOI 10.1007/s10562-013-1100-9

Ce-Promoted Rh/TiO_2 Heterogeneous Catalysts Towards Ethanol Production from Syngas

Changming Li · Junmin Liu · Wa Gao · Yufei Zhao · Min Wei

Received: 4 July 2013 / Accepted: 30 August 2013 / Published online: 25 September 2013

Abstract Direct synthesis of ethanol from syngas derived from coal, natural gas, or biomass is one of the most promising routes for renewable energy production. In this work, Ce-promoted highly-dispersed Rh catalyst on TiO_2 support was prepared by the deposition–precipitation method, which exhibits largely enhanced catalytic activity and selectivity for ethanol production from syngas. XRD and TEM reveal a high dispersion of Rh nanoparticles ($\sim$1 nm) on the surface of TiO_2 support by the introduction of CeO_2. It was found that the relative content of Rh and CeO_2 imposes significant influence on the catalytic behavior, and the sample of 1 wt% Rh–1 wt% CeO_2/TiO_2 exhibits the highest CO conversion (32 %) and the largest ethanol selectivity (33 %) under the conditions of 573 K, 3 MPa, H_2:CO = 2:1. H_2-TPR and XPS results confirm a gradually enhanced electron interaction between Rh and CeO_2 with the increase of Ce content; CO-TPD further reveals that the Rh–CeO_2 interaction generates a new adsorption site for CO, accounting for the improved selectivity towards ethanol. Therefore, this work provides a facile and effective method for the preparation of Rh–CeO_2/TiO_2 catalysts with high catalytic behavior, which can be potentially used in syngas conversion to ethanol.

Keywords Syngas conversion · Ethanol production · Rh–CeO_2/TiO_2 Catalysts

C. Li · J. Liu · W. Gao · Y. Zhao · M. Wei (✉)
State Key Laboratory of Chemical Resource Engineering, Beijing University of Chemical Technology, Beijing 100029, People's Republic of China
e-mail: weimin-hewei@163.com; weimin@mail.buct.edu.cn

1 Introduction

The limited resources of fossil fuels and environmental concerns have stimulated a broad intensive search for alternative energy sources [1, 2]. Ethanol, as a renewable and clean fuel, has attracted increasing attention [3, 4]. The catalytic ethanol production from syngas, which can be conveniently manufactured from natural gas, coal and biomass, [5] becomes one of the most prospective technologies in the new energy fields. Despite the immense amount of research concentrated on this catalytic conversion process, no commercial process exists due to the challenging chemical and technological barriers [6]. The key is to develop efficient catalysts towards ethanol production for practical industrial applications. Rh-based catalysts supported on SiO_2 have been known to be the most efficient ones in the synthesis of C2 oxygenates from CO hydrogenation due to their unique CO adsorption behavior [7–14]. Their catalytic activity/selectivity can be further improved by introducing promoters in Rh catalysts such as Fe [15], Mn [16], La [17] and V [18]. Although much progress has been made, a main obstacle in these Rh-based catalysts is their relatively low efficiency for commercial process. Therefore, how to achieve cost-effective Rh-based catalysts with superior activity and selectivity towards ethanol synthesis from syngas remains a challenging goal.

Supported catalysts on reducible metal oxides (e.g., TiO_2) exhibit remarkably enhanced performance in many catalytic processes, including hydrogenation, [19] partial oxidation, [20] or reforming reaction [21]. The amphoteric oxide TiO_2 (isoelectric $IEP_{TiO2} = 6$) with rich hydroxyl group would guarantee a high metal dispersity by the deposition–precipitation method, which provides an efficient way to prepare highly-dispersed metal catalysts compared with the conventional impregnation process [22–

25]. On the other hand, it has been reported that the incorporation of promoters into the Rh-based catalysts plays a key role in generating required active sites for the selective synthesis of C2 oxygenates [26–28]. Ceria serves as an effective rare-earth promoter owing to its unique 4f electronic structure [29–32]. This motivates us to combine the specific merits of both TiO_2 and CeO_2 to fabricate Ce-promoted Rh/TiO_2 catalytic materials with improved performance in syngas conversion. In addition, the clarification of Rh-promoter interaction is crucial for understanding and designing new catalysts, although it is still of great difficulty.

In this work, a series of highly-dispersed 1 wt% Rh–*x* % CeO_2/TiO_2 catalysts were prepared by the method of deposition–precipitation, which show largely-enhanced catalytic behavior for ethanol production from CO hydrogenation. The relative content of CeO_2 imposes significant influence on the catalytic behavior of Rh–CeO_2/TiO_2, and the best catalytic performance was obtained over the sample of 1 wt% Rh–1 wt% CeO_2/TiO_2 with CO conversion of 32 % and ethanol selectivity of 33 % under the following condition: 573 K, 3 MPa, H_2:CO = 2:1. X-Ray diffraction (XRD), TEM, H_2-TPR, XPS, and CO-TPD characterization techniques were further performed to study the metal-promoter (Rh–CeO_2) interaction of these 1 wt% Rh–*x* % CeO_2/TiO_2 catalysts in detail. It is found that an electron interaction occurs at the Rh–CeO_2 boundary interface, which serves as active sites for ethanol production. A moderate Rh–CeO_2 interaction maximizes the quantity of the active sites, accounting for the best catalytic performance observed over 1 wt% Rh–1 wt% CeO_2/TiO_2.

2 Experimental Section

2.1 Materials

The TiO_2 (P25; specific surface area: 52 m^2/g), $RhCl_3 \cdot 3H_2O$ and $Ce(NO_3)_3 \cdot 9H_2O$ were purchased from Sigma-Aldrich. Deionized water was used in all the experimental processes.

2.2 Catalyst Preparation

A series of supported catalysts, 1 wt% Rh–*x* % CeO_2/TiO_2 ($x = 0, 0.5, 1, 2, 5, 10$), were prepared using the deposition–precipitation method. Na_2CO_2 was used as precipitant owing to its advantage in preparation of homogeneous small metal particles with low loading [22–25]. Before preparation, TiO_2 was previously dried in air at 120 °C for at least 12 h. Typically, for the sample of 1 wt% Rh–1 wt% CeO_2/TiO_2, 1 g of TiO_2 was added to 80 mL of an aqueous solution containing $RhCl_3$ (1.21 mM) and $Ce(NO_3)_3$ (0.89 mM) precursor. $Rh(OH)_3$ and $Ce(OH)_3$ was exclusively precipitated on the surface of support by the slow addition of Na_2CO_3 (1 M) solution until the pH reached to 8.0. The resultant solid was filtered and washed thoroughly with deionized water until no chloride ion was detected in the filtrate (tested by $AgNO_3$ solution). The solid obtained was dried at 120 °C for 12 h, followed by calcination in air at 400 °C for 4 h. Subsequently, the sample was treated by flowing H_2 at 300 °C for 3 h for further catalytic reaction and characterization.

2.3 Catalyst Characterization

XRD patterns of samples were obtained on a Shimadzu XRD-6000 diffractometer, using Cu Kα radiation ($\lambda = 0.154$ nm) at 40 kV, 30 mA, a scanning rate of $5°min^{-1}$, a step size of $0.02°s^{-1}$, and a 2θ angle ranging from 10 to 90°. High resolution transmission electronmicroscopy (HRTEM) was carried on a JEM-3010 at an accelerating voltage of 200 kV. X-ray photoelectron spectra (XPS) were recorded on a Thermo VG ESCALAB250 X-ray photoelectron spectrometer at a pressure of 2×10^{-9} Pa using Al K_α X-ray as the excitation source. Temperature-programmed reduction (H_2-TPR) was carried out in a quartz reactor at atmospheric pressure. 100 mg of sample was loaded in the middle of the reactor tube which was purged with N_2 at 200 °C for 2 h. Then a reductive gas (5 vol% H_2/Ar) was introduced at a flow rate of 40 mL/min. The temperature of the reactor was augmented linearly from 30 to 600 °C with a ramp of 10 °C/min by a temperature-programmed controller. CO-TPD was carried out on a Micromeritics TPD/TPR 2910 AutoChem instrument. The catalysts were pre-reduced in flowing 10 vol% H_2–Ar at 300 °C for 2 h, cooled to ambient temperature, and flushed with Ar until the baseline was steady. CO was desorbed by heating the samples from 20 to 500 °C at a rate of 5 °C/min in flowing Ar.

2.4 Catalytic Evaluation

Carbon monoxide hydrogenation reaction was carried out in a fixed bed stainless steel tubular microreactor (8 mm in diameter, 500 mm in length). The temperature of the reactor was controlled via a temperature controller. H_2, CO and N_2 were purged into the reactor at a desired rate by mass flow controllers. Nitrogen was used as an internal standard gas in the reactor feed. The catalyst (0.3 g) mixed with silicon carbide (1.5 g) was loaded into the reactor and reduced in situ in a flow of H_2 (40 mL/min) under atmospheric pressure at 300 °C for 2 h. Subsequently, the syngas with a flow rate of 40 mL/min (H_2:CO = 2.0, v/v) was introduced to increase the pressure to 3 MPa. The composition of the outlet gas stream was determined using an

online GC-2014C Shimadzu gas chromatograph equipped with a Porapak Q column and a TCD detector. Liquid products were captured using an ice-water bath and analyzed off-line with the same chromatograph (a PEG-20 M capillary column and a FID detector) or GC–MS (Shimadzu, 2010) analysis.

CO conversion (X_{CO}) and product distribution of S_i were calculatedaccording to the following equations:

$$X_{CO} = \frac{molesCO_{in} - molesCO_{out}}{molesCO_{in}} \times 100\% \quad (1)$$

$$S_i = \frac{molesP_i}{\sum_{i=1}^{n} moleP_i} \times 100\% \quad (2)$$

where P_i is the mole number of product i.

3 Results and Discussion

3.1 Structural and Morphological Characterization of Rh–CeO_2/TiO_2 Catalysts

The detailed information for the as-synthetized catalysts (content, specific surface area) is summarized in Table 1. It can be seen that the Rh and Ce loading in these products are rather close to the feed ones. For BET measurements, the specific surface area increased with the elevated Ce content in the catalysts. Figure 1 displays the XRD patterns of various 1 wt% Rh–*x* % CeO_2/TiO_2 samples after reduced at 300 °C for 2 h, with P25 as a reference sample. The XRD pattern of P25 (Fig. 1a) shows representative reflections of titanium oxide (Anatase: 25.3°, 37.8° and 48.0°; Rutile: 27.9° and 36.4°). For the 1 wt% Rh–*x* % CeO_2/TiO_2 samples with *x* % increasing from 0 to 10 %, only the reflections of TiO_2 phase were observed (Fig. 1b–g). No characteristic XRD diffraction peaks for both Rh and CeO_2 were observed, indicating that these species are amorphous or highly-dispersed on the surface of P25 with rather small particle size (below the detection limit of XRD).

Table 1 The detailed information for the as-synthetized 1 wt% Rh–*x* % CeO_2/TiO_2 catalysts

Samples	Nominal content (wt%) (Rh, Ce)	Determined content (wt%) (Rh, Ce)[a]	Specific surface area/ (m^2/g^{-1})[b]
1 wt% Rh/TiO_2	1.00, 0.00	0.98, 0.01	52.1
1 wt% Rh–0.5 wt% CeO_2/TiO_2	1.00, 0.50	0.99, 0.46	55.1
1 wt% Rh–1 wt% CeO_2/TiO_2	1.00, 1.00	0.94, 0.95	54.2
1 wt% Rh–2 wt% CeO_2/TiO_2	1.00, 2.00	1.02, 1.96	58.9
1 wt% Rh–5 wt% CeO_2/TiO_2	1.00, 5.00	0.96, 5.03	62.7
1 wt% Rh–10 wt % CeO_2/TiO_2	1.00, 10.00	0.97, 10.08	65.1

[a] Determined by ICP measurement

[b] Determined by BET measurement

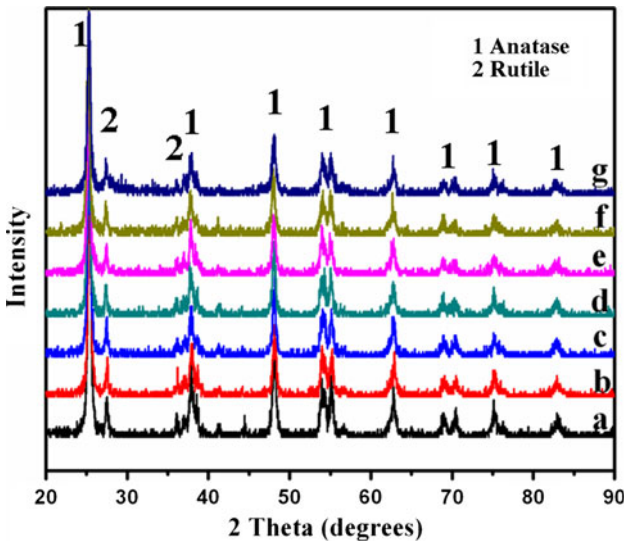

Fig. 1 XRD patterns of **a** P25, **b** 1 wt% Rh/TiO_2, **c** 1 wt% Rh–0.5 wt% CeO_2/TiO_2, **d** 1 wt% Rh–1 wt% CeO_2/TiO_2, **e** 1 wt% Rh–2 wt% CeO_2/TiO_2, **f** 1 wt% Rh–5 wt% CeO_2/TiO_2, **g** 1 wt% Rh–10 wt% CeO_2/TiO_2

The morphology features of the 1 wt% Rh–*x* % CeO_2/TiO_2 catalysts were further revealed by TEM (Fig. 2). Numerous small dots were observed on TiO_2 support with rather high dispersion in the samples from 1 wt%Rh/TiO_2 (Fig. 2a) to 1 wt% Rh–5 wt% CeO_2/TiO_2 (Fig. 2e), which can be attributed to Rh nanoparticles according to the 0.22 nm lattice spacing. Interestingly, the particle size of Rh decreases from 1.5 to 0.9 nm as the Ce content increases from 0 to 5 wt% (Fig. 2, inset: the Rh size distribution was calculated over more than 200 nanoparticles). No CeO_2 phase was observed in these five samples due to its low content and the relative contrast for CeO_2 and TiO_2 in TEM observation. In the case of 1 wt% Rh–10 wt% CeO_2/TiO_2 however, even no Rh nanoparticles were detected by TEM owing to the very small particle size, but CeO_2 nanoparticles appear with the size range 2–4 nm. Based on the XRD and TEM results, it can be concluded that highly-dispersed 1 wt% Rh–*x* % CeO_2/TiO_2 catalysts were successfully synthetized by the deposition–precipitation method.

3.2 The Study on the Interaction Between Rh and CeO_2 in Rh–CeO_2/TiO_2 Catalysts

The hydrogen temperature programmed reaction (H_2-TPR) measurements were carried out to give key information on

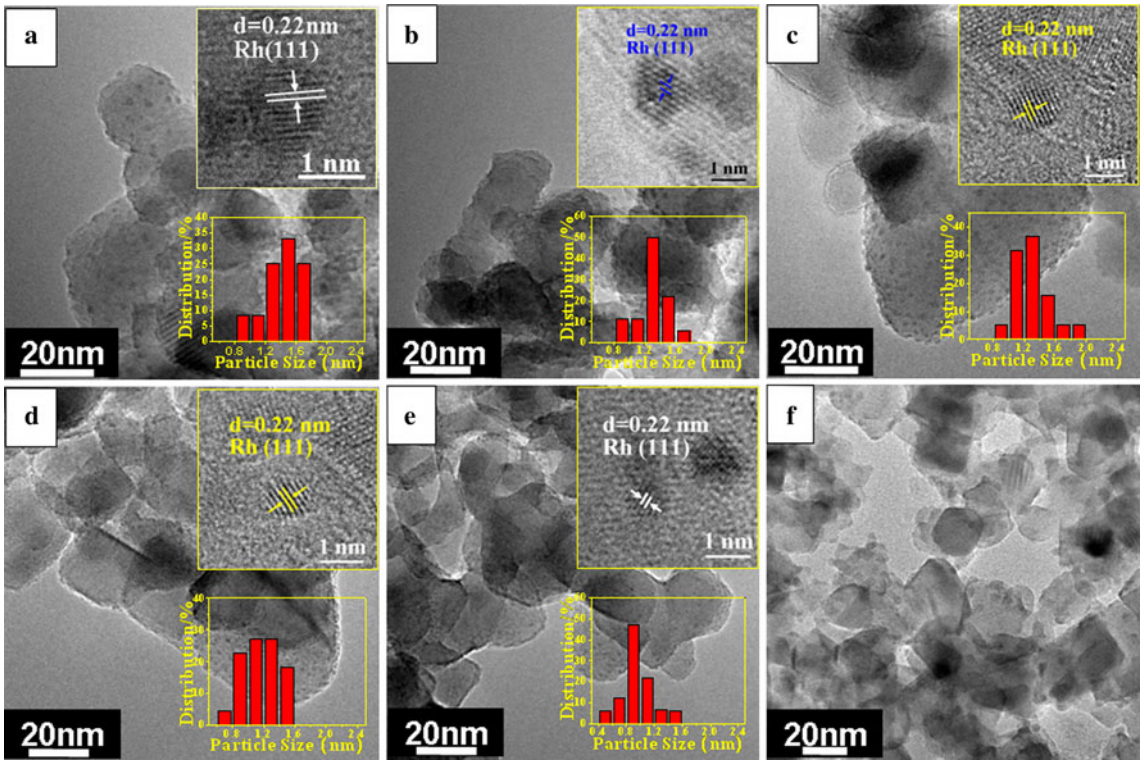

Fig. 2 TEM images of **a** 1 wt% Rh/TiO_2, **b** 1 wt% Rh–0.5 wt% CeO_2/TiO_2, **c** 1 wt% Rh–1 wt% CeO_2/TiO_2, **d** 1 wt% Rh–2 wt% CeO_2/TiO_2, **e** 1 wt% Rh–5 wt% CeO_2/TiO_2, **f** 1 wt% Rh–10 wt% CeO_2/TiO_2. The *inset* shows the size distribution and the HRTEM image of supported Rh nanoparticles

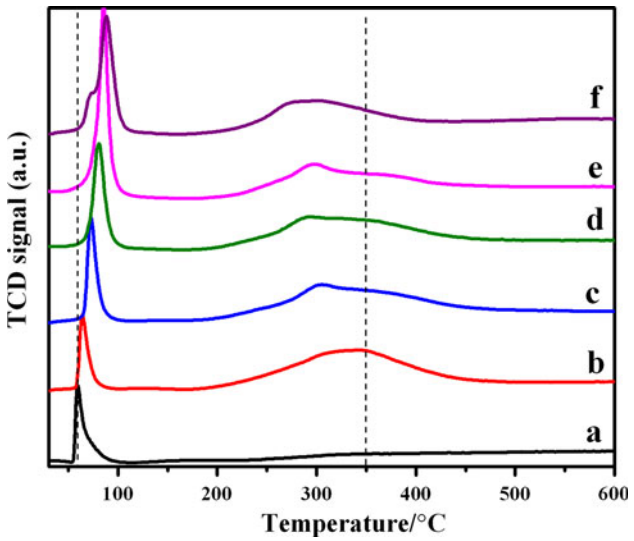

Fig. 3 TPR profiles of **a** 1 wt% Rh/TiO_2, **b** 1 wt% Rh–0.5 wt% CeO_2/TiO_2, **c** 1 wt% Rh–1 wt% CeO_2/TiO_2, **d** 1 wt % Rh–2 wt % CeO_2/TiO_2, **e** 1 wt% Rh–5 wt% CeO_2/TiO_2, **f** 1 wt% Rh–10 wt% CeO_2/TiO_2

the redox property of Rh and CeO_2 species on TiO_2. Fig. 3 demonstrates the comparative H_2-TPR study of the 1 wt% Rh–*x* % CeO_2/TiO_2 catalysts with different Ce content. The 1 wt% Rh/TiO_2 sample without CeO_2 shows a single peak at 58.6 °C, corresponding to the reduction of Rh_2O_3 to metallic Rh^0 (Fig. 3a) [33, 34]. The introduction of CeO_2 improves the reduction temperature of supported Rh species: with the enhancement of CeO_2 content from 0.5 to 10 wt %, the reduction peak of Rh_2O_3 increases from 64.2 to 88.5 °C gradually (Fig. 3b–f). In addition, multiplicity of reduction peaks was observed in the temperature region 280–400 °C. The amount of H_2 consumed in this process largely exceeds the theoretical one for total reduction of bare Rh_2O_3, suggesting the reduction of surface CeO_2 [34, 35]. It's interesting to see that the main reduction peak temperature of CeO_2 decreases from 338.9 to 285.1 °C as the loading of CeO_2 increases from 0.5 to 10wt % (Fig. 3b–f), which shows an opposite change tendency compared with that of Rh species. This indicates that Rh^0 can effectively activate H_2 molecules, which subsequently spillover to the surface of CeO_2 and promote its reduction [36, 37]. The gradually increasing and decreasing reduction temperature for Rh_2O_3 and CeO_2, respectively, indicate the enhanced interaction between Rh and CeO_2 species. The decreased Rh particle size from 1 wt% Rh/TiO_2 to 1 wt% Rh–10 wt% CeO_2/TiO_2 sample (Fig. 2) may enlarge the Rh–CeO_2 boundary interface, resulting in the enhanced interaction [38, 39]. Based on the HRTEM and ICP results, the Rh species exists in its metallic state in these catalysts,

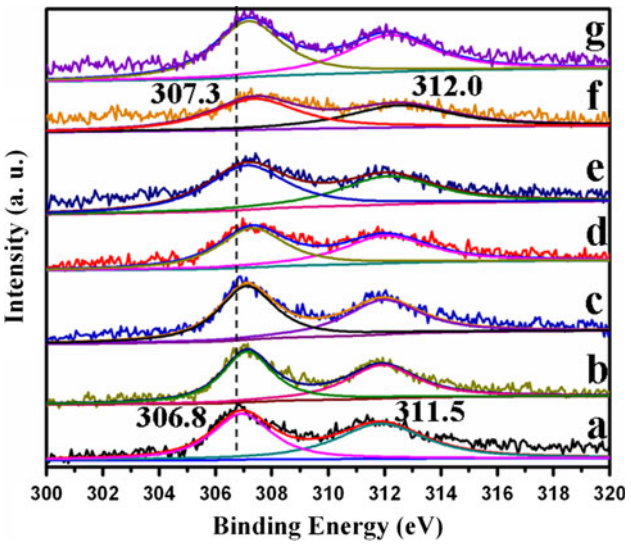

Fig. 4 The spectra of Rh 3d XPS in catalysts: **a** 1 wt% Rh/TiO_2, **b** 1 wt% Rh–0.5 wt% CeO_2/TiO_2, **c** 1 wt% Rh–1 wt% CeO_2/TiO_2, **d** 1 wt% Rh–2 wt% CeO_2/TiO_2, **e** 1 wt% Rh–5 wt% CeO_2/TiO_2, **f** 1 wt% Rh–10 wt% CeO_2/TiO_2, **g** the used 1 wt% Rh–1 wt% CeO_2/TiO_2

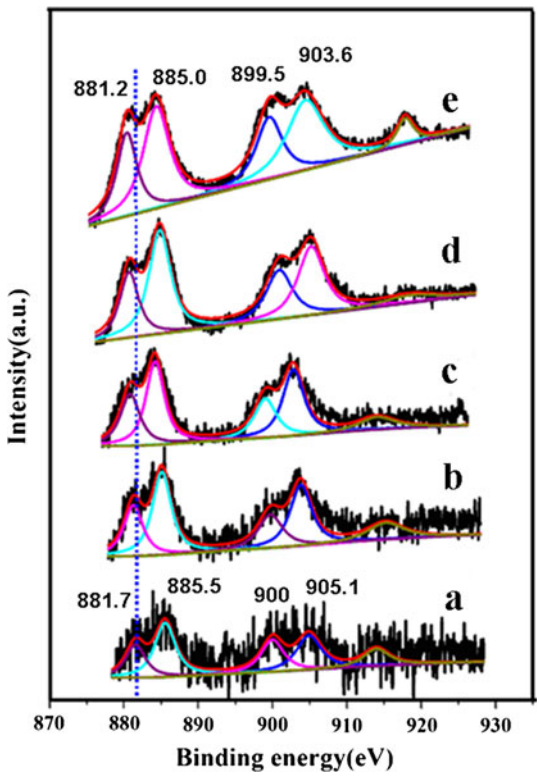

Fig. 5 The spectra of CeO_2 3d XPS in catalysts: **a** 1 wt% Rh–0.5 wt% CeO_2/TiO_2, **b** 1 wt% Rh–1 wt% CeO_2/TiO_2, **c** 1 wt% Rh–2 wt% CeO_2/TiO_2, **d** 1 wt% Rh–5 wt% CeO_2/TiO_2, **e** 1 wt% Rh–10 wt% CeO_2/TiO_2

and the Rh–CeO_2 interaction may be attributed to the electron transfer or oxygen transfer between metal and reducible oxide [35, 40].

To get further insights into the chemical state of Rh and Ce species on TiO_2 and their interaction, X-ray photoelectron spectra (XPS) were performed for the series reduced 1 wt% Rh–*x* % CeO_2/TiO_2 samples. All the samples were transferred to a XPS chamber as soon as possible to avoid the exposure in air after reduction by H_2. The survey 3d XPS spectra for Rh and Ce are displayed in Fig. 4, Fig. 5, respectively, all of which are referenced to the residual carbon at the binding energy of 284.6 eV. For the sample of 1 wt% Rh/TiO_2 (Fig. 4a), two peaks observed at 306.8 and 311.5 eV could be attributed to Rh($3d_{5/2}$) and Rh($3d_{3/2}$) of metallic Rh^0 [41]. The introduction of CeO_2 in 1 wt% Rh–*x* % CeO_2/TiO_2 samples slightly increases the Rh 3d bind energy from 306.9 and 311.6 eV (Fig. 4b) to 307.2 and 311.9 eV (Fig. 4f), along with the enhancement of CeO_2 loading. In addition, the Rh 3d XPS spectrum of the used 1 wt% Rh–1 wt% CeO_2/TiO_2 catalyst (Fig. 4g) shows no obvious change compared with the fresh one (Fig. 4c), indicating that the electronic structure properties can be maintained after catalytic test. On the other hand, two peaks at 881.7 and 900.0 eV assigned to Ce($3d_{5/2}$) and Ce($3d_{3/2}$) of CeO_2 are observed in the 1 wt% Rh–0.5 wt% CeO_2/TiO_2 sample (Fig. 5a), [42]. and these bind energy values decreases gradually to 811.2 and 899.5 eV in the sample of 1 wt% Rh–10 wt% CeO_2/TiO_2 (Fig. 5e). The opposite change tendency of Rh and Ce 3d XPS bind energies suggests an enhanced electron transfer from Rh to CeO_2 with the increase of CeO_2 loading, accounting for the improved Rh–CeO_2 interaction from 1 wt% Rh/TiO_2 to 1 wt% Rh–10 wt% CeO_2/TiO_2 as observed by the H_2-TPR characterization.

The incorporation of promoter may impose great influence on the adsorption properties, therefore, CO-TPD measurements were also carried out to investigate the CO adsorption/desorption on these catalyst (Fig. 6). For 1 wt% Rh/TiO_2, three CO desorption peaks are observed in different temperature range: low temperature site (at ~100 °C, denoted as CO_α), medium temperature (MT) site (at ~200 °C, denoted as $CO_{\beta1}$), and high temperature (HT) site (at ~400 °C, denoted as CO_γ), which can be assigned to CO desorbed at Rh surface, Rh/TiO_2 boundary interface and TiO_2 surface, respectively, according to the previous reports [43, 44]. The introduction of CeO_2 gradually decreases the desorption peak intensity for CO_α at Rh surface gradually from 1 wt% Rh/TiO_2 (Fig. 6, curve a) to 1 wt% Rh–10 wt% CeO_2/TiO_2 (Fig. 6, curve f); while the the HT CO_γ peak intensity increases slightly due to the CO absorbed on CeO_2 surfac [45]. Most importantly, it is worthy noting that a new MT desorption peak ($CO_{\beta2}$) at ~150 °C appears for the 1 wt% Rh–0.5 wt% CeO_2/TiO_2 sample (Fig. 6, curve b), which can be assigned to

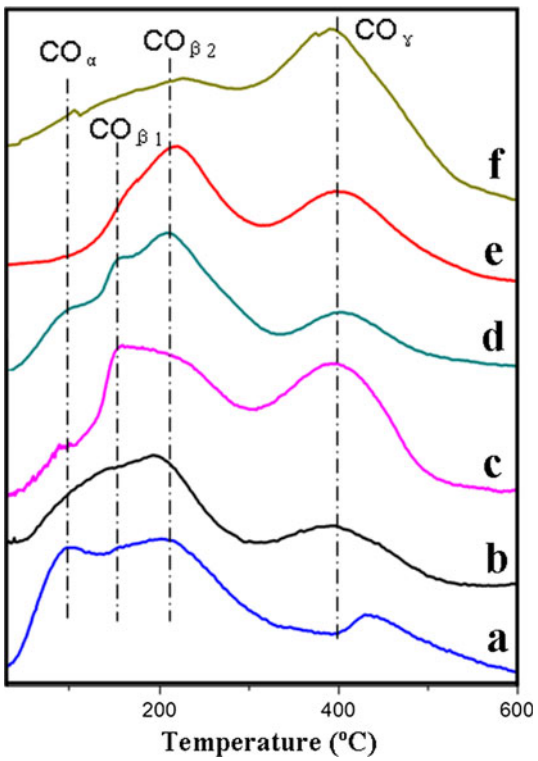

Fig. 6 CO-TPD curves of **a** 1 wt% Rh/TiO_2, **b** 1 wt% Rh–0.5 wt% CeO_2/TiO_2, **c** 1 wt% Rh–1 wt% CeO_2/TiO_2, **d** 1 wt% Rh–2 wt% CeO_2/TiO_2, **e** 1 wt% Rh–5 wt% CeO_2/TiO_2, **f** 1 wt% Rh–10 wt%CeO_2/TiO_2

desorption at Rh/CeO_2 boundary interface. This peak intensity increases to its maximum value in the 1 wt% Rh–1 wt% CeO_2/TiO_2 sample (Fig. 6, curve c), and then fades away with further increase of CeO_2 loading (Fig. 6, curve f). Based on the results of TEM, TPR and XPS, it is proposed that the electron interaction between Rh and CeO_2 leads to new active sites at the Rh/CeO_2 boundary interface, which is responsible for the new MT desorption peak at ~50 °C ($CO_{\beta 2}$). Moreover, the moderate Rh–CeO_2 interaction in the 1 wt% Rh–1 wt% CeO_2/TiO_2 sample results in the maximum of the MT CO absorbed sites ($CO_{\beta 2}$).

3.3 Evaluation of Catalytic Performances

The catalytic performance of the 1 wt% Rh–*x* % CeO_2/TiO_2 catalysts towards CO hydrogenation for ethanol production was evaluated under the following reaction conditions: 4.0 MPa, 573 K, GHSV of 2000 h^{-1}, n (H_2)/n (CO) = 2.0. Figure 7; Table 2 show the time-on-stream (TOS) behavior of CO conversion and the corresponding product distribution on these catalysts, respectively. It can be observed from Fig. 7 that the introduction of Ce as promoter dramatically increases the CO conversion in comparison with the 1 wt% Rh/TiO_2 sample, and the

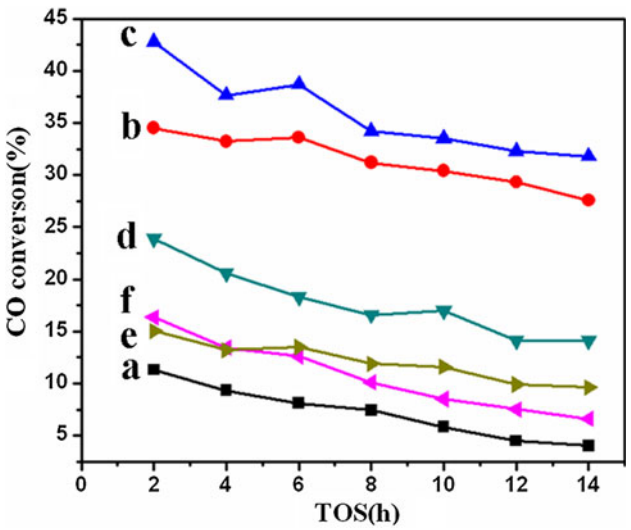

Fig. 7 CO conversion rate versus TOS for **a** 1 wt% Rh/TiO_2, **b** 1 wt% Rh–0.5 wt% CeO_2/TiO_2, **c** 1 wt% Rh–1 wt% CeO_2/TiO_2, **d** 1 wt% Rh–2 wt% CeO_2/TiO_2, **e** 1 wt% Rh–5 wt% CeO_2/TiO_2, **f** 1 wt% Rh–10 wt% CeO_2/TiO_2

maximum CO conversion (32 %) was achieved for 1 wt% Rh–1 wt% CeO_2/TiO_2 catalyst after the catalystic performance was steady more than 14 h. However, a further increase in Ce-loading leads to decreased CO catalytic conversion, especially in the case of 1 wt% Rh–10 wt% CeO_2/TiO_2 (only ~4.1 % conversion, 14 h). The selectivity for methanol/ethanol obeys a similar tendency, and the 1 wt% Rh–1 wt% CeO_2/TiO_2 catalyst also displays the highest selectivity (33 %) towards ethanol among these catalysts. The results demonstrate that an appropriate Rh/CeO_2 ratio is crucial for obtaining the highest C_2H_5OH formation activity. In addition, it can be also seen that the CeO_2-promoted Rh catalysts show significant suppression of the formation of methane from 69.47 % (1 wt% Rh/TiO_2) to 46.63 % (1 wt% Rh–1 wt% CeO_2/TiO_2), which is an undesired low-value product. Based on the HRTEM, XPS and CO-TPD results, the new MT CO adsorption site at ~150 °C ($CO_{\beta 2}$) derived from the Rh–CeO_2 electronic interaction could be recognized as the active site for the catalytic CO hydrogenation process, and the maximum of this active site over the 1 wt% Rh–1 wt% CeO_2/TiO_2 sample accounts for the best catalytic behavior towards syngas conversion. The activity and selectivity towards ethanol production over 1 wt% Rh–1 wt% CeO_2/TiO_2 catalyst in this work is comparable to the most reported Rh catalysts catalysts [6, 46–48]. Moreover, the rather low loading of Rh (1 %) in this work is another main advantage from the viewpoint of effective utilization of noble metals. The demonstrated excellent activity and selectivity of 1 wt% Rh–1 wt% CeO_2/TiO_2 makes it serve as a promising candidate for catalytic ethanol production from syngas.

Table 2 Catalytic performance of 1 wt% Rh–*x* % CeO_2/TiO_2 catalysts

Catalysts	CO conversion (%)	Selectivity (%)					
		CH_4	C_{2+} HC[a]	MeOH	EtOH	C_{2+} oxy[b]	CO_2
1 wt% Rh/TiO_2	5.54	69.47	3.64	5.19	13.55	2.25	5.90
1 wt% Rh–0.5 wt% CeO_2/TiO_2	30.91	61.72	3.28	6.47	21.47	4.16	2.90
1 wt% Rh–1 wt% CeO_2/TiO_2	32.24	46.63	2.17	11.32	33.32	4.67	1.89
1 wt% Rh–2 wt% CeO_2/TiO_2	17.61	53.69	3.55	8.56	24.44	4.34	5.42
1 wt% Rh–5 wt% CeO_2/TiO_2	11.51	64.38	3.74	5.47	15.38	3.52	7.51
1 wt% Rh–10 wt% CeO_2/TiO_2	9.23	65.41	3.82	7.68	16.56	3.33	3.20

Reaction condition: 3 MPa, 300 °C, GHSV = 2,400 h^{-1}, $n(H_2)/n(CO) = 2$

[a] Hydrocarbons with 2 or more carbons

[b] Oxygenates with 2 or more carbons excluding ethanol

4 Conclusions

In summary, a series of CeO_2-promoted Rh/TiO_2 catalysts with low Rh loading (1 wt%) were prepared by the deposition–precipitation method, which exhibit largely enhanced catalytic activity and selectivity towards ethanol production from syngas. The XRD and TEM results reveal Rh nanoparticles with size of $\sim$1 nm are highly dispersed on the TiO_2 surface by the introduction of CeO_2. A gradually enhanced electron interaction between Rh and CeO_2 occurs along with the increase of CeO_2 content, as confirmed by H_2-TPR and XPS. The CO-TPD results further suggest that the Rh–CeO_2 interaction generates a new adsorption site for CO, and the maximum amount of this site can be obtained over 1 wt% Rh–1 wt% CeO_2/TiO_2 sample with a moderate Rh–CeO_2 interaction. The best catalytic performance can be achieved over the 1 wt% Rh–1 wt% CeO_2/TiO_2 sample with CO conversion of 32 % and ethanol selectivity of 33 % under the following conditions: 573 K, 3 MPa, H_2:CO = 2:1, making it as a promising candidate for catalytic ethanol production from syngas.

Acknowledgments This work was supported by the 973 Program (Grant No. 2011CBA00504), the National Natural Science Foundation of China (NSFC) and the Beijing Natural Science Foundation (2132043). M. Wei particularly appreciates the financial aid from the China National Funds for Distinguished Young Scientists of the NSFC.

References

1. Spivey JJ, Egbebi AA (2007) Chem Soc Rev 36:1514
2. Hu BS, Fujimoto K (2009) Catal Lett 129:416
3. Rostrup-Nielsen JR (2005) Science 308:421
4. Yang Y, Wang YD, Liu S, Song QY, Xie ZK, Gao Z (2009) Catal Lett 127:448
5. Ahmed A, Lewis RS (2007) Biotechnol Bioeng 97:1080
6. Mei DH, Rousseau R, Kathmann SM, Glezakou VA, Engelhard MH, Jiang W, Wang C, Gerber MA, White JF, Stevens DJ (2010) J Catal 271:325
7. Hanaoka T, Arakawa H, Matsuzaki T, Sugi Y, Kanno K, Abe Y (2000) Catal Today 58:271
8. Fan ZL, Chen W, Pan XL, Bao XH (2009) Catal Today 147:86
9. Mo X, Gao J, Goodwin JG Jr (2009) Catal Today 147:139
10. Gao J, Mo X, Chien AC, Torres W, Goodwin JG Jr (2009) J Catal 262:119
11. Ho S, Su Y (1997) J Catal 168:51
12. Basu P, Panayotov D, Yates JT Jr (1998) J Am Chem Soc 110:2074
13. Solymosi F, Tombacz I, Kocsis M (1982) J Catal 75:78
14. Jiang DH, Ding YJ, Pan ZD, Chen WM, Luo HY (2009) Catal Lett 121:241
15. Luo HY, Lin PZ, Xie SB, Zhou HW, Xu CH, Huang SY, Lin LW, Liang DB, Yin PL, Xin Q (1997) J Mol Catal A 122:115
16. Hu JL, Wang Y, Cao CS, Elliott DC, Stevens DJ, White JF (2007) Catal Today 120:90
17. Gao J, Mo X, Chien AC, Torres W, Goodwin JG Jr (2009) J Catal 262:119
18. Mo X, Gao J, Goodwin JG Jr (2009) Catal Today 147:139
19. Li CM, Zhang ST, Zhang BS, Su DS, He S, Zhao YF, Liu J, Wang F, Wei M, Evans DG, Duan X (2013) J Mater Chem A 1:2461
20. Green IX, Tang W, Neurock M Jr, Yates JT (2012) J Am Chem Soc 134:13569
21. Martinez LM, Araque TM, Vargas JC, Roger AC (2013) Appl Catal B 132:499
22. Zanella R, Giorgio S, Henry CR, Louis C (2002) J Phys Chem B 106:7634
23. Balaraju M, Rekha V, Prabhavathi Devi BLA, Prasad RBN, Sai Prasad PS, Lingarah N (2010) Appl Catal A 384:107
24. Rio ED, López-Haro M, Cies JM, Delgado JJ, Calvino JJ, Trasobares S, Blanco G, Cauqui MA, Bernal S (2013) Chem Commun 49:6722
25. Torres C, Campos C, Fierro JLG, Oportus M, Reyes P (2013) Catal Lett 143:763
26. Burch R, Hayes MJ (1997) J Catal 165:249
27. Ojeda M, Granados ML, Rojas S, Terreros P, Garcia–Garcia FJ, Fierro JLG (2004) Appl Catal A 261:47
28. Boffa A, Lin C, Bell AT, Somorjai GA (1994) J Catal 149:149
29. Chang HZ, Li JH, Yuan J, Chen L, Dai Y (2013) Catal Today 201:139
30. González AV, Karatzas X, Pettersson LJ (2013) Fuel 107:162
31. Zuo SF, Du YJ, Liu FJ, Han D, Qi CZ (2013) Appl Catal A 451:65
32. Lu YJ, Li S, Guo LJ (2013) Fuel 103:193
33. González AV, Karatzas X, Pettersson LJ (2013) Fuel 107:162
34. Huang L, Choong C, Chen LW, Wang Z, Zhong ZY, Campos-Cuerva C, Lin JY (2013) Chem Cat Chem 5:220

35. Wang R, Xu HY, Liu XB, Ge QJ, Li WZ (2006) Appl Catal A 305:204
36. Bernal S, Calvina JJ, Cifredo GA, Rodreguez-Izquierdo JM, Perrichon V, Laachir A (1992) J Catal 137:1
37. Trovarelli A, de Leitenburg C, Dolcetti G, Lorca JL (1995) J Catal 151:111
38. Kim SS, Lee SJ, Hong SC (2011) Chem Eng J 169:173
39. Miyazawa T, Okumura K, Kunimori K, Tomishige K (2008) J Phys Chem C 112:2574
40. Vayssilov GN, Lykhach Y, Migani A, Staudt T, Petrova GP, Tsud N, Skála T, Bruix A, Illas F, Prince KC, Matolín V, Neyman KM, Libuda J (2011) Nat Mater 10:310
41. Parres-Esclapez S, Such-Basañez I, Illán-Gómez MJ, Le Salinas-Martínez Lecea C, Bueno-López A (2010) J Catal 276:390
42. Force C, Roman E, Guil JM, Sanz J (2007) Langmuir 23:4569
43. Constantiou DA, Álvarez-Galván MC, Fierro JLG, Efstathiou AM (2012) Appl Catal B 117:81
44. Egbebi A, Schwartz V, Overbury SH, Spivey JJ (2010) Catal Today 149:91
45. Xu J, Mullins DR, Overbury SH (2006) J Catal 243:158
46. Mo XH, Gao J, Umnajkaseam N, Goodwin JG Jr (2009) J Catal 267:167
47. Haider MA, Gogate MR, Davis RJ (2009) J Catal 261:9
48. Gogate MR, Davis RJ (2009) Chem Cat Chem 1:295